Microstructure and Phase Composition in High-Strength Aluminium Alloys Produced by A Splat-Cooling Technique

Joachim Kinder and Eduard Arzt

(Max-Planck-Institut für Metallforschung, Institut für Werkstoffwissenschaft, Seestr. 92, D-7000 Stuttgart 1, and Institut für Metallkunde der Universität Stuttgart, Stuttgart)

Dedicated to Prof. Dr. rer. nat. Dr. h.c. mult. Günter Petzow on the occasion of his 65th birthday

Rapid solidification (RS) experiments have been carried out on high-strength AlZnMgCuX alloys (X = Zr, Ti, Cr or Mn) using the rotating-wing splat-cooling technique. The resulting particles ("splats") were examined by light-microscopy, X-ray diffraction (Guinier-technique) and TEM. In comparison to industrially produced powders the microstructure was refined by about a factor of two. The alloying elements could be kept partially in solution and/or led to metastable phases which precipitated during solidification or handling before subsequent examination. Heat treatment of the rapidly solidified splats generated a relatively homogeneous and dense precipitation of several metastable and/or stable phases. In some cases the RS technique used could not prevent special high-melting phases from precipitating already in the melt. These phases acted as quite effective grain size stabilizers during subsequent heat treatment. The higher solidification rates are concluded to show potential for improving the mechanical properties of these alloys.

Gefüge und Phasenbestand in mit der Splat-Cooling-Technik hergestellten hochfesten Aluminium-Legierungen

An hochfesten AlZnMgCuX-Legierungen (X = Zr, Ti, Cr oder Mn) wurden mit einer Drehflügel-Apparatur Schnellerstarrungsexperimente durchgeführt. Die daraus resultierenden Partikel („Splats") wurden lichtmikroskopisch, röntgenographisch (Guinier-Verfahren) und mit TEM untersucht. Im Vergleich zu industriell hergestellten Pulvern war das Gefüge ungefähr um den Faktor 2 feiner. Die Legierungselemente konnten teilweise im Festkörper gelöst gehalten werden und/oder führten zu metastabilen Phasen, die sich während der Erstarrung oder noch vor den nachfolgenden Untersuchungen ausschieden. Die Wärmebehandlung der schnellerstarrten Splats erzeugte eine relativ homogene und dichte Ausscheidung mehrerer metastabiler und/oder stabiler Phasen. In einigen Fällen konnte die Schnellerstarrungstechnik nicht die Ausscheidung spezieller hochschmelzender Phasen bereits in der Schmelze unterbinden. Diese Ausscheidungen wirkten als Korngrößestabilisatoren während der nachfolgenden Wärmebehandlung. Insgesamt ergibt sich durch Schnellerstarrung ein Potential zur Verbesserung der mechanischen Eigenschaften dieser Legierungen.

1 Introduction

The principal advantages of applying rapid solidification techniques to metallic alloys are well known even if retaining these benefits in technical production routes is often difficult. In a joint industry – institute project which was concerned with the development of high-strength aluminium alloys by powder metallurgy the question arose whether or not the use of more powerful laboratory methods for rapid solidification would improve the microstructure of materials with identical composition as industrially produced powders in a useful and technically promising way. To answer this question a rotating-wing splat-cooling equipment was adapted and the effects of cooling rates as high as 10^7 K/s on the microstructure were studied.

2 Experimental

2.1 Alloys

The compositions of the alloys on which rapid solidification experiments were carried out are listed in Table 1. The alloys were produced by a project partner (VAW-Bonn) and supplied in the form of extruded rod sections. This "as-received" starting material was remelted and then subjected to the splat-cooling experiments.

2.2 Splat-Cooling Technique

A rotating-wing splat-cooling apparatus, developed and described by Predel[1]), was used. Especially for specimens containing elements with high partial vapour-pressures (e.g. Li, Mg or Zn containing alloys) at or above their liquidus temperatures, some modifications of the equipment were necessary to minimize selective evaporation losses during melting and subsequent rapid solidification under vacuum ($1.3 \cdot 10^{-3}$ Pa).

Inside the wall of a boron-nitride crucible a sheathed thermocouple was mounted for qualitative temperature record and for temperature control of the process. This construction protected the thermocouple from attack by the aggressive melt. The crucible was covered by a specially designed mica plate (muscovite). This cover helped to minimize, but was not able to totally preclude, vapour losses of particular elements. Additionally the losses could be limited by minimizing the holding time of the melt before it was atomized into the evacuated recipient by an external argon-gas pulse. The mica plate also prevented the melt from levitating into the upper parts of the graphite susceptor, which was externally heated through an induction coil.

Inside the chamber a wing made of a creep-resistant copper alloy rotates at 10000 rpm and strikes through the cloud of molten droplets, which on contact solidify rapidly in the form of flattened "splats". It is obvoius that the time for complete solidification is inversely related to the splat dimensions: qualitatively the smallest and thinnest splats will have experienced the highest cooling rates. For TEM preparation it was convenient to achieve a minimum diameter of 3 mm.

Every "shot" produced about 50 splats with diameters between 0.5 and 5 mm and a thickness in the range from

Table 1. Compositions (at.%) of the Al alloys investigated, balance Al (A = as-received, Q = as-quenched, T = heat treated).

name	nominal composition	condition	Cu	Mg	Zr	Ti	Zn	Cr	Mn
40	Al 9 Zn 3 Mg 1.5 Cu 1.5 Zr	A	1.54	3.03	1.56	–	7.01	–	–
		Q	1.73	2.57	1.67	–	3.20	–	–
		T	1.81	2.64	1.73	–	3.21	–	–
41	Al 9 Zn 3 Mg 1.5 Cu 1.5 Ti	A	1.47	3.22	–	1.52	8.79	–	–
		Q	1.57	2.96	–	1.58	7.43	–	–
		T	1.57	3.06	–	1.49	7.53	–	–
42	Al 9 Zn 3 Mg 1.5 Cu 4.0 Cr	A	1.46	3.29	–	–	8.95	4.17	–
		Q	1.63	3.47	–	–	8.05	3.29	–
		T	1.69	2.93	–	–	5.14	3.76	–
43	Al 9 Zn 3 Mg 1.5 Cu 4.0 Mn	A	1.50	3.33	–	–	8.93	–	3.78
		Q	1.60	2.90	–	–	5.20	–	3.81
		T	1.93	2.62	–	–	3.50	–	3.94

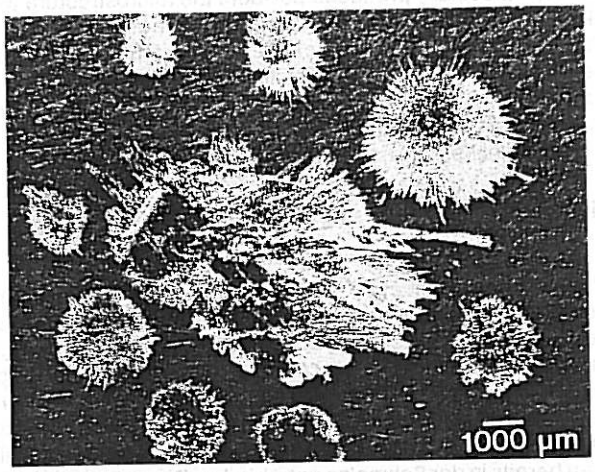

Fig. 1. Appearance of some typical splats.

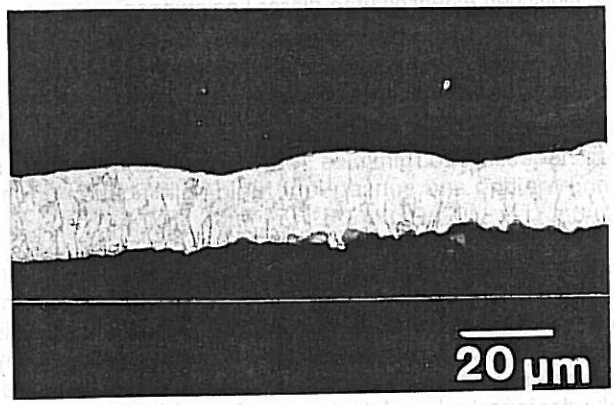

Fig. 2. Cross-section of a splat, exhibiting the typical columnar microstructure which resulted from the growth direction in course of the temperature gradient between the cold substrate and the solidifying droplet.

150 down to 5 μm. Figures 1 and 2 show some examples of splats and a typical cross-section. The average size of the splats could be influenced by the diameter of the outlet in the bottom of the crucible, the over-pressure of the Ar pulse and, through the viscosity of the melt, by the degree of super-heating.

The intensity of contact between the droplet and the copper-alloy substrate has a decisive influence on the rate of heat removal during rapid solidification[2]). Faster heat removal leads to a higher undercooling of the melt, which solidifies heterogeneously from the melt – substrate contact. In this sense the intensity of the contact could be controlled principally by the velocity of the rotating wing. To achieve the highest cooling rates all but a few experiments were carried out using the fastest rotating velocity.

2.3 Heat Treatment and Analysis

To allow a valid comparison with industrially produced powders, which normally have to be degassed by a heat treatment, a similar thermal exposure (with maximum temperature 480 °C for 0.5 h) was applied to the rapidly solidified splats. To prevent the hot splats from oxidizing, they were sealed in a glass ampoule filled with argon gas. Because of possible evaporation losses it was necessary to determine the elemental composition of each run using atomic absorption spectroscopy (AAS) and, especially for Zr, the inductive coupled plasma (ICP) technique. Table 1 shows the results of these analyses for each experimental stage.

The phase composition of the alloys before and after the experiments was determined by the X-ray Guinier technique using Cu-Kα_1 radiation. The "as-received" starting material was ground to powder, while the splats could be analysed directly without being crushed because of their relatively small thickness. For TEM investigations, the splats were electrolytically thinned using a Struers Tenupol twin-jet apparatus and the electrolyte "A8" containing perchloric acid. The thinned splats were examined in a TEM (JEOL 200A and 200CX) in both the as-quenched and heat treated state. Because of inhomogeneous thinning response, TEM observations were sometimes problematic and resulted in micrographs of varying quality.

2.4 Determination of the Cooling Rate

In practice there is no reliable way to measure cooling rates exceeding 10^6 K/s (which is a typical value for the melt-spinning technique). Fortunately the microstructure

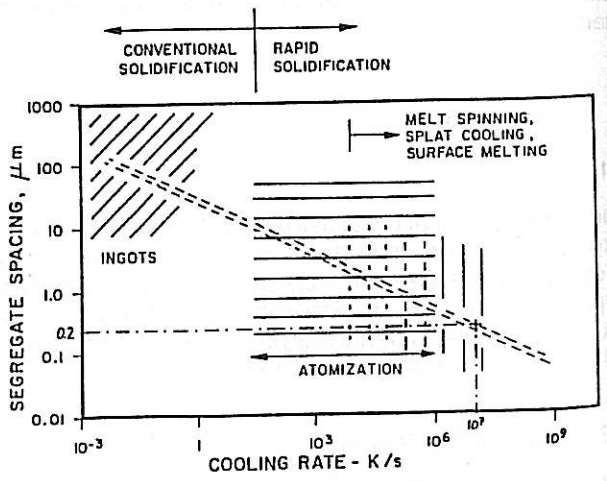

Fig. 3. Segregate spacing vs. cooling rate for Al alloys[7]).

Table 2. Phases in the different high-strength Al alloys (results of XRD and TEM) (A = as-received, Q = as-quenched, T = heat treated).

state	method	40 (Zr-containing)	41 (Ti-containing)	42 (Cr-containing)	43 (Mn-containing)
A	XRD	α_{ss} Zn_2Zr Zr_3Si_2 Mg_2Si Mg_2Zn_3 ? AlCuMg ? Al_7Cu_2Fe? no Al_3Zr!	α_{ss} $MgZn_2$ AlCuMg (2 modifications) Al_3Mg_2 Al_3Ti ?	α_{ss} $Al_{18}Cr_2Mg_3$ AlCuMg	α_{ss} Al_6Mn $MgZn_2$
Q	XRD	α_{ss} Al_3Zr (tetr., stable) further phase?	α_{ss} Al_3Ti (tetr., stable) $AlTi_2$	α_{ss} (2x) $Al_{13}Cr_2$	α_{ss} Al_6Mn AlMn ? $MgZn_2$?
	TEM	elongated (0.6 µm) → Al_3Zr very fine, rounded esp. in cell-boundaries (20 nm) → ?	rounded (50 nm) → Al_3Ti? very fine, rounded (5 nm) → $AlTi_2$	rounded (0.05 - 0.3 µm) → $Al_{13}Cr_2$	quasi-crystals very fine in cell-boundaries (5 nm) → Al_6Mn
T	XRD	α_{ss} Al_3Zr (tetr., stable) MgZn Zr_3Si_2 ? AlCuMg ?	α_{ss} $MgZn_2$ AlCuMg (2 modifications) Al_3Mg_2 Al_3Ti ?	α_{ss} $Al_{18}Cr_2Mg_3$ AlCuMg	α_{ss} Al_6Mn $MgZn_2$ (2 modifications) (Al, Fe, Si)
	TEM	elongated, faceted (0.6 µm) → Al_3Zr very fine, rounded (20 nm) → MgZn?	needle-like faceted (200 nm) → $MgZn_2$ very fine faceted (60 nm) → AlCuMg ?	faceted, twinned (0.1 µm) → $Al_{18}Cr_2Mg_3$ very fine-grained (50 nm) → AlCuMg	elongated, oriented intergrown lamell. (1-2 µm) → G",T ? facett. (0.3 µm) → Al_6Mn facett. (0.1 µm) → $MgZn_2$? very fine, rounded (<10 nm) → (Al, Fe, Si) ?

of an alloy often shows some unique features which can be correlated approximately with the solidification velocity (for example see Kurz[3]). Frequently the secondary dendrite-arm spacing (DAS) is used as a measure for cooling rates. Sometimes however – as in our case – the cooling rates are too high for the formation of secondary dendrites. The higher solidification-front velocity instead produces solidification cells accompanied by lateral segregation. Following for example Matya[4]), Couper[5]) and Samuel[6]), it seems reasonable in these cases to treat the average diameter of the cells as equivalent to the DAS and thus to estimate the cooling rate from this type of segregation spacing (Fig. 3)[7]). This approach was adopted in the present work. Note that such cooling rate estimates can only be rough approximations as no consideration is given to the influence of the additional alloying elements.

3 Results and Discussion

3.1 X-ray Diffraction Analysis

Figure 4 shows the results of the X-ray diffraction analysis (XRD). For each alloy type the as-received starting condition (designated "A") can be compared with one or two rapid solidification runs (designated "Q") and the subsequently heat-treated state ("T"). The X-ray interferences of the as-received starting condition are broadened; this is caused by mechanical distortion during the grinding for specimen preparation.

In the as-quenched state nearly all splats, except for the Mn containing variant, show more or less pronounced increases in lattice spacings of the solid solution, which is obviously due to supersaturation effects. The fact that interferences are broadened in the as-quenched condition indicates a certain inhomogeneity of the structural parameters in the as-quenched state, perhaps in the form of an

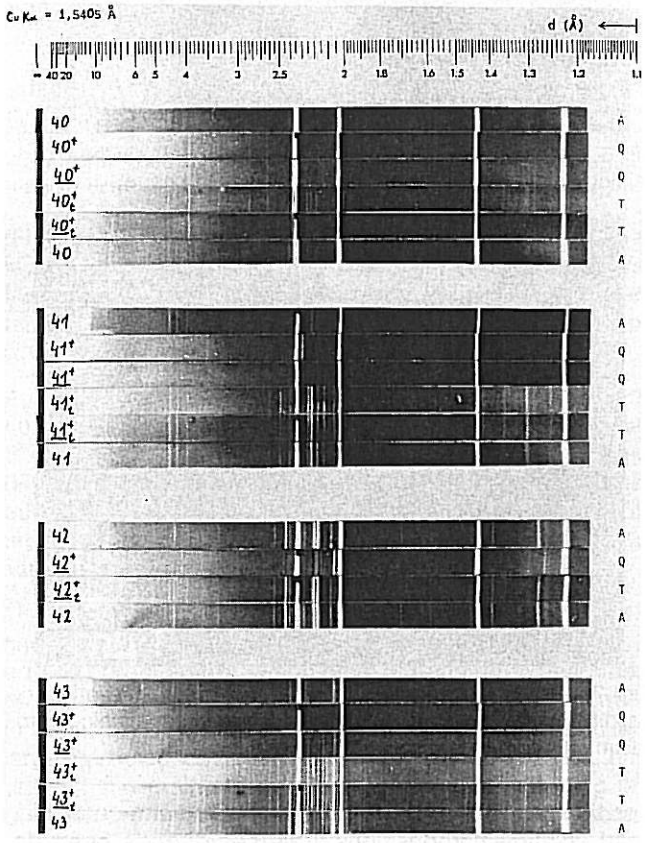

Fig. 4. X-ray diffraction patterns of all alloy variants in different states ("A" = as-received starting condition, "Q" = as-quenched, "T" = heat treated).

inhomogeneous distribution of the alloying elements or because of quenched-in vacancies.

The as-quenched Cr containing alloy exhibits in addition a doubling of the higher order interferences due to a decom-

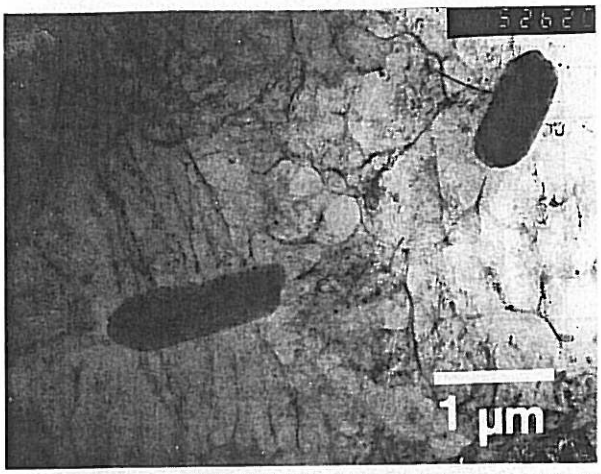

Fig. 5. TEM-image (bright field) of Zr containing as-quenched splat, exhibiting solidification-cells which are arranged around a coarse primary Al_3Zr-precipitate.

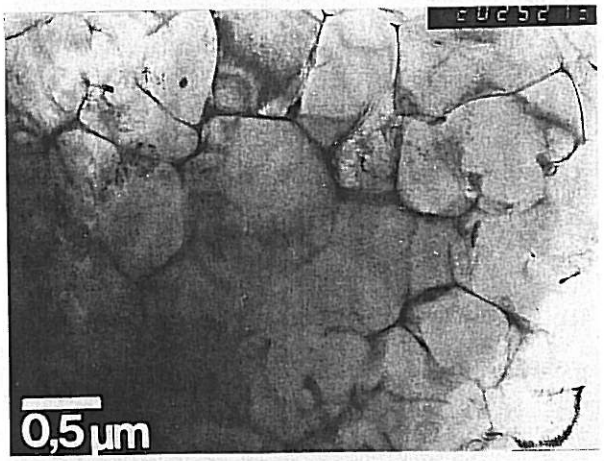

Fig. 6. Solidification cells and very fine precipitates in the Ti containing as-quenched variant (TEM-bright field image).

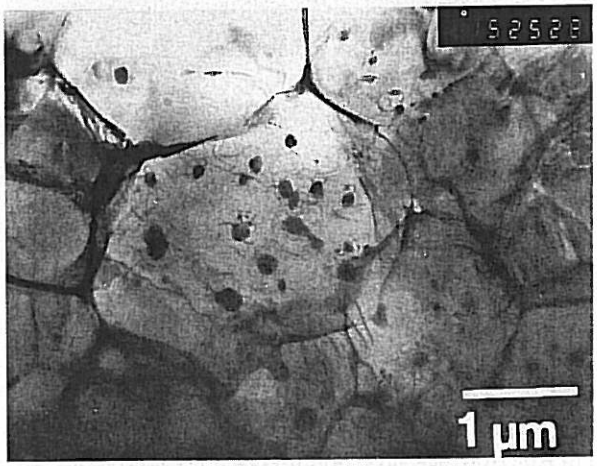

Fig. 7. Unfaceted precipitates with dislocation networks and solidification cells in the as-quenched variant, containing chromium (TEM-bright field image).

position reaction into two different chromium containing solid solution compositions. This has already been described[8]) for splat-cooled binary Al-Cr alloys containing more than 2.3 at.% (≈ 1.2 wt.%) chromium.

In all cases the rapid solidification led to significantly decreased amounts of precipitated phases compared to the starting condition, which can be regarded to be near the equilibrium state. After annealing the quenched splats, qualitatively the same phase composition re-appeared.

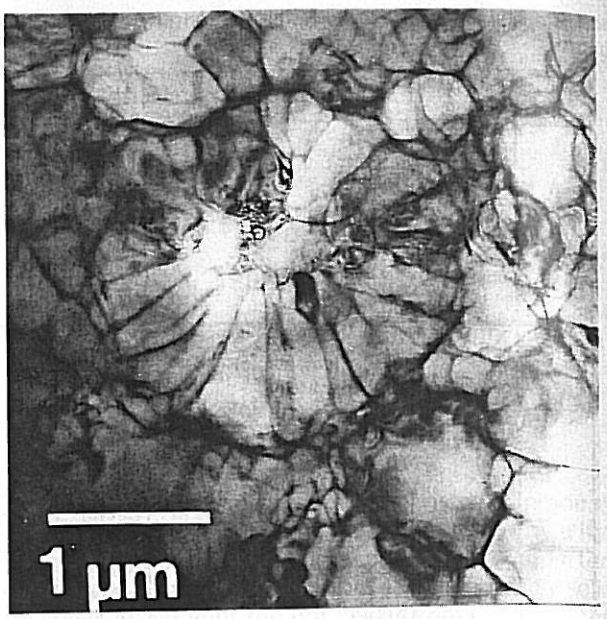

Fig. 8. Special arrangement of the solidification cells ("quasi-crystal") in an as-quenched splat of the Mn containing alloy (TEM bright field image).

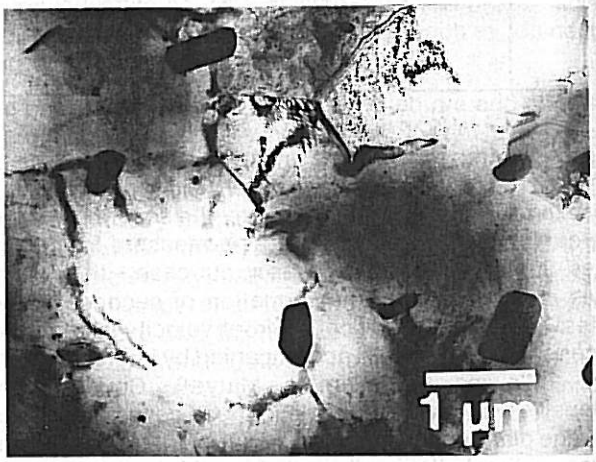

Fig. 9. Heat treated splat of the Zr containing alloy exhibiting a fine-grained microstructure due to the coarse Al_3Zr precipitates which pinned the moving grain boundaries thus inhibiting grain coarsening (TEM bright field image).

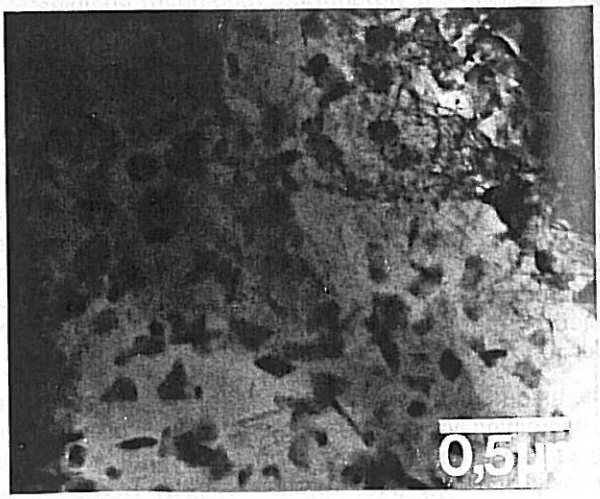

Fig. 10. Relatively dense and homogeneous distribution of precipitates in a heat treated splat of the Ti containing alloy (TEM bright field image).

The phases identified by X-ray diffraction in all specimens are listed in Table 2, which also includes the results obtained by TEM for comparison.

Especially for the Zr and Ti containing alloys another observation has to be pointed out. Due to the relatively low maximum temperature of the melt (≦ 1000 °C) which was limited by our equipment, high-melting equilibrium phases (e.g. Al_3Zr, Al_3Ti with melting points of 1580 °C and 1340 °C, respectively) precipitated in the melt and remained in the solid state during quenching. Only at much higher processing temperatures total solutioning of these stable phases could be achieved, albeit at the expense of selective vapour-losses in our apparatus.

3.2 TEM Investigation

The TEM investigations revealed for nearly all splats in the as-quenced state a cellular solidification structure with average cell diameters smaller than 1.0 μm (Figs. 5, 6 and 8). Only the chromium containing splats (Fig. 7) had coarser cells with typical diameters of up to 2.5 μm. With the aid of Fig. 3 the cooling rate in the present study would be estimated as 10^4 K/s in the Cr containing alloy and up to 10^7 K/s in the other alloys.

Because the experimental conditions of each run were kept almost constant, the chromium obviously has to be responsible for this significant deviation. According to Warlimont[8]) this effect can be explained in terms of a special super-saturation effect. As long as the chromium is retained in solid solution, the microstructure exhibits cell sizes varying between 0.5 and 1 μm. If the chromium content exceeds the solubility of the matrix (≈ 2.3 at.% for a cooling rate of 10^6 K/s), remarkable differences in the cell sizes, ranging from typically 10 μm to 1 μm, will occur due to the presence of small clusters of solute atoms or of vacancies.

A second possible explanation for the deviating cooling rate of the Cr variant is the following. The addition of Cr to aluminium raises the liquidus temperature drastically from about 660 °C to roughly 840 °C for a binary Al-4 wt.% Cr alloy[9]). Even if the additional alloying elements may reduce this effect in the present case, it seems reasonable to assume that the superheating of this variant was not sufficiently high, thus leading to an increased viscosity which also has a decisive influence on the cooling rate[2]). An indication for this effect is the presence of precipitates in the as-quenched state. These unfaceted precipitates associated with dislocation networks (Fig. 7) are thought to be $Al_{13}Cr_2$ particles according to the X-ray analysis (JCPDS: 29–14).

The Zr containing alloy exhibits relatively large precipitates which are slightly faceted and appear to act as embryos for crystallisation (Fig. 5). X-ray diffraction revealed them to be Al_3Zr precipitates. The very fine and rounded precipitates visible in Fig. 5 were too small and appeared too seldom for the analysis by the available techniques.

For the Ti containing alloy the phases identified by X-ray diffraction were partly visible in the examined regions of the splat. As Fig. 6 reveals, the cellular microstructure contains a very dense precipitation of rather small particles (ø ≧ 10 nm) which were identified as Al_3Ti (JCPDS: 26–39).

The rapidly solidified Mn containing variant features a special morphology of the cellular microstructure. The solidification cells are often arranged in a "rosette" manner

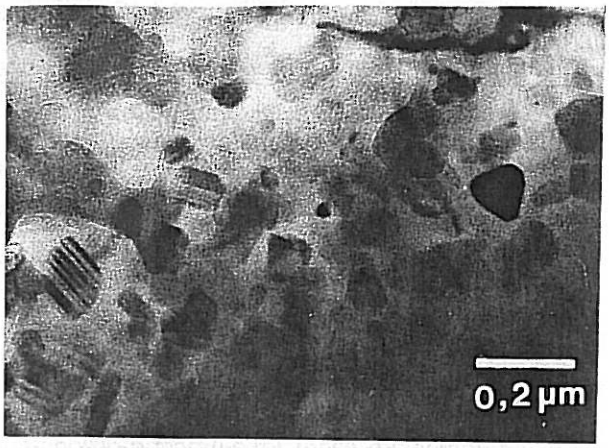

Fig. 11. Homogeneous distribution of a frequently twinned phase which precipitated after heat treatment in the Cr containing alloy (TEM bright field image).

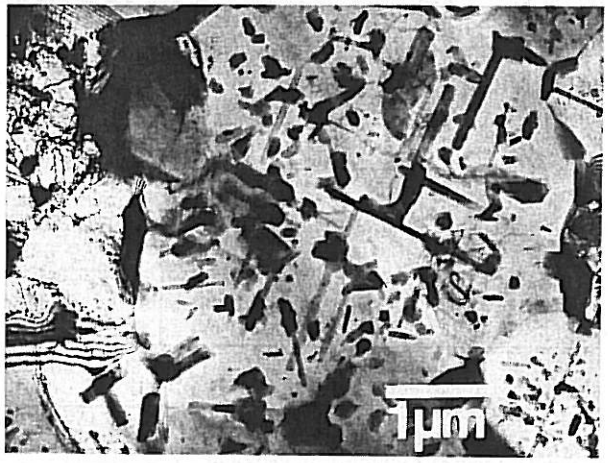

Fig. 12. Heat treated splat of the Mn containing variant exhibiting several types of precipitates which partly grew in an oriented manner with respect to the matrix (TEM bright field image).

(Fig. 8). In accordance with the results of microstructural investigations of rapidly quenched Mn containing alloys, for instance by Shechtman[10]) or by Pennetier[11]), this arrangement of the cellular microstructure is reminiscent of "quasi-crystals".

After heat treatment, all specimens except the zirconium containing variants exhibited a homogeneous and relatively dense distribution of newly precipitated phases (Figs. 9 to 12). The metastable cellular structure of the as-quenched state transformed into a grain structure with different grain sizes depending on the alloy type (see Table 3).

The microstructure of the Zr containing alloy remained fine-grained (ø 1 to 2 μm) during heat treatment. The faceted Al_3Zr precipitates, which have already been described for the as-quenched state, are now preferentially located at the newly developed grain boundaries. These relatively large particles obviously pin the grain boundaries and prevent the grains from coarsening excessively (Fig. 9). Furthermore two types of precipitates were found: rounded, with a diameter of about 20 nm, and elongated, with a length of about 20 nm. The results of the XRD analysis identified them as Zn_2Zr (JCPDS: 17–75) and MgZn (JCPDS: 8–206), respectively.

The alloy variant containing titanium revealed after heat treatment a very homogeneous precipitation of plate-like hexagonal $MgZn_2$ (JCPDS: 34-457) in a matrix with an average grain diameter of roughly 3 μm (Fig. 10).

Table 3. Comparison of the microstructures produced by splat-cooling (this paper) and gas-atomization of powders[13] (d = grain or cell diameter).

state	40 (Zr-containing)	41 (Ti-containing)	42 (Cr-containing)	43 (Mn-containing)
gas-atomized	← solidification-cells →			
	d = 1.5 μm	d = 1.5 - 2 μm	d = 0.5 - 1 μm	d = 0.5 - 1 μm
	no precipitates visible	no precipitates visible	precipitates - rounded ~ 0.5 μm	precipitates - rounded ~ 0.5 μm
as-quenched splats	← solidification-cells →			
	d ≤ 1.5 μm	d = 0.5 - 1 μm	d = 1 - 2.5 μm	d ≤ 0.5 μm
	← precipitates →			
	- elongated 0.7 - 1μm - rounded 15 - 50 nm	- rounded 10 - 50 nm	- rounded 0.2 μm	at cell-boundaries (very fine)
degassed gas-atomized powders	← grain-size exceeds the size of the photograph (d > 5 μm) →			
	← precipitates →			
	elongated 0.1-0 .5 μm	- rounded 0.2-0.5 μm	- rounded 0.3 -0.3 μm	- plate-like 0.2 μm - plate-like 0.6 μm
in the same manner heat-treated splats	grain-structure d ≤ 2μm	grain-structure d ≤ 3 μm	grain-size exceeds the size of the photograph (d ≥ 2.5 μm)	grain-structure d ≤ 4 μm
	← precipitates →			
	- elongated, faceted partly at grain-boundary triples ≤ 0.7 μm - decorated subgrain-boundaries < 10nm	- faceted ≤ 0.2 μm	very dense precipitation - faceted and frequently twinned ≤ 0.1 μm	very dense precipitation - plate-like ~ 1.5 μm - lath-like, oriented intergrown ~ 0.1 μm - rounded < 0.2 μm - rounded ~ 15 nm

The chromium alloyed variant exhibited a high volume fraction of an apparently cubical, frequently twinned phase, with sizes of about 0.1 μm, within the solid solution which has a grain size close to 2.5 μm (Fig. 11). X-ray diffraction determined these precipitates to be $Al_{18}Cr_2Mg_3$ (JCPDS: 29–18).

The metastable "quasi-crystals" in the as-quenched Mn variant disappeared completely during heat treatment. In a slightly coarser grained matrix ($\varnothing \leqq 4$ μm) at least three different precipitation species could now be distinguished (Fig. 12): $MgZn_2$ (JCPDS: 34–457) which precipitated in a fine ($\varnothing \approx 10$ nm) and homogeneous manner; much coarser (typical size 0.1 to 0.3 μm) and rounded or sometimes faceted Al_6Mn (JCPDS: 6–665) seems to be the main precipitate; in addition, one can observe very large particles which are oriented with respect to the matrix and show an internal lamellar structure. A very similar phase was reported in Mn containing alloys and designated as G″ ($\approx \Phi$-$Al_{10}Mn_3$; hexagonal) by Nes[12]. Its lamellar structure was ascribed to the presence of stacking faults. They regarded this phase as a metastable precursor to Al_6Mn and found it to grow parallel to low-index directions in the matrix.

The simultaneous occurrence of thermodynamically stable and metastable phases both in the as-quenched and the heat treated state of all the alloys examined is an indication of a special state of imbalance. Table 3 contains a comparison of the microstructures produced by splat-cooling with those of gas atomized powders[13]) of identical composition. Splat-cooling led to microstructures roughly half in size compared to the gas atomized state. Thus, it can be inferred from Fig. 3 that the cooling rate during splat-cooling was about one or two orders of magnitude higher than during the atomization process. The precipitates in the splat-cooled state were normally very fine and often located at cell boundaries. A significant deviation was shown by the Zr containing alloy. The non-suppressable Al_3Zr precipitates acted as grain growth inhibitors resulting in a very small grain size after heat treatment.

The quite homogeneous and dense precipitation of different phases in the other alloy types after annealing seems to be a direct result of the higher cooling rates, which obviously increased the solubility of the alloying elements. After heat treatment this supersaturation led to a very dense precipitation of several stable and metastable phases. Compared to the heat treated gas atomized powders the grain sizes of the splats remained relatively small (Table 3).

Overall, it appears that a very rapidly quenched alloy can be a promising precursor for achieving microstructures with interesting features, which do not disappear completely during heat treatment. The homogeneous distribution of precipitates, be they thermodynamically stable or metastable after heat treatment, and the resulting relatively small grain sizes constitute an attractive improvement of the microsctructure over conventional powder processing. The question remains, however, whether these possible benefits can be retained during powder metallurgical processing of splat-like material.

4 Conclusions

1) Splat-cooling of high-strength Al alloys with cooling rates of up to 10^7 K/s allowed refined microstructures to be produced, with solidification cells roughly half in size compared to gas atomized powders of the same alloy composition.

2) The solubility for the alloying elements of the alloys investigated was extended, which resulted in a finer and more homogeneous distribution of precipitates after annealing. Certain precipitates which cannot be suppressed even during rapid solidification were found to be very effective in restricting grain growth during subsequent annealing.

3) If the benefits of the splat-cooling process over conventional gas atomization of powders, i.e. the refinement of grain size and precipitate distribution, can be retained during processing, the higher cooling rates could have the potential of improving the mechanical properties of high-strength aluminium alloys.

The authors wish to express their gratefulness to Prof. Predel and Prof. Sommer, who gave permission to use their splat-cooling apparatus for these experiments and valuable advice. The authors are also grateful to VAW, Bonn, for supply of the starting material. This work was sponsored by the German Ministry of Research and Technology (project number 03M0009GO).

Literature

1) B. PREDEL, G. DUDEK, Z. Metallkde. **69** (1978) 773–776.
2) F. SOMMER, J. WACHTER, Int. J. Rapid Solidification **3** (1988) 223–236.
3) W. KURZ, D. J. FISCHER, Fundamentals of Solidification, 2nd Ed., Trans. Techn Publ., Aedermansdorf (1986).
4) H. MATYA, B. C. GIESSEN, N. J. GRANT, J. Inst. Metals **96** (1968) 30–32.
5) M. J. COUPER, PM Aerospace Materials, Vol. 1, MPR Publishing Service Ltd., Shrewsbury (1984) 28/1–28/10.
6) F. H. SAMUEL, Metall. Trans. A **17A** (1986) 73–91.
7) M. COHEN, M. C. FLEMINGS, Rapidly Solidified Crystalline Alloys, The Metallurgy Society, Inc., Warrendale (1985) 1–23.
8) H. WARLIMONT, W. ZINGG, P. FURRER, Mat. Sci. Engg. **23** (1976) 101–105.
9) F. KING, Aluminium and its Alloys, John Wiley & Sons, New York (1987).
10) D. SHECHTMAN, R. J. SCHAEFER, F. S. BIANCIANIELLO, Metall. Trans. A **15A** (1984) 1987–1997.
11) J. PENNETIER, J. M. DUBOIS, C. JANOT, A. BILDE, Phil. Mag. B **55** (1987) 435–457.
12) E. NES, S. E. NAESS, R. HOIER, Z. Metallkde. **63** (1972) 248–252.
13) G. LÜTJERING, D. HELM, A. GYSLER, 3rd Internal Progress-Report of the Joint Industry – Institute Project (1987).

(Eingegangen am 4. Januar 1991)